The Damage Process Monitoring in Structures with Quasi-Brittle behavior in the perspective of Complex System

EWSHM 2024
11th European Workshop on Structural Health Monitoring

The Damage Process Monitoring in Structures with Quasi-Brittle behavior in the perspective of Complex System

Ignacio ITURRIOZ[1], Boris N. Rojo TANZI[1], Angelica COLPO[1], Leandro FRIEDRICH[2], Ediblu CESAR[3] ,Giuseppe LACIDOGNA[3].
[1]Department of Mechanical Engineering, Federal University of Rio Grande do Sul (UFRGS), Porto Alegre/RS90046-902, Brazil, ignacio@mecanica.ufrgs.br
[2]Departament of Mechanical Engineering, Federal University of Pampa, Av. Tiaraju 810, Alegrete CEP 97546-550, Brazil.
[3]Department of Structural, Geotechnical and Building Engineering, Politecnico di Torino, Turin 10129, Italy.

Abstract The damage process in structures with quasi-brittle behavior, such as concrete, rocks, ceramics, and composites, is characterized by typical phenomena including sensitivity to size effect, the interaction of micro-fissures, and the transition of the continuum to discontinuity through the so-called localization effect. There are many approaches to modeling the mechanical behavior of this type of material/structure. Our simulation strategy, which is a version of the discrete element model, aligns with Prof. Krajcinovic's perspective. According to him, the random nature of the material is a key aspect that must due to consider. With the aim of addressing this problem, the Acoustic Emission Technique (AET) could also be useful to characterize the damage process. The spatial and temporal distribution of events during the damage process is determined by the combination of signals captured from different locations in the structure. This information can be used to calculate global parameters and their evolution during structural damage. These parameters may serve as precursors to identify local or global damage. It is worth noting that structure failure can be viewed as a phase transformation phenomenon. The Renormalization Group Theory, proposed by Wilson, and Anderson's ideas related to complex systems provide a theoretical perspective that allows us to understand the collapse in solids from a different angle. The present work considers some applications related to the characterization of the damage process of quasi-brittle structures/materials, carried out by our research group. We aim to establish a link between these results and the ideas of Wilson and Anderson.

Keywords: Acoustic Emission Technique, Discrete Element Method, critical phenomena

Media and Publishing Partner
https://doi.org/10.58286/29711

1. Introduction

The damage process in quasi-brittle materials, such as concrete, rocks, ceramics, and several artificial composite materials, is characterized by the interaction among a cluster of micro-cracks, localization effect, and size effect. The way to the collapse system is governed by the damage in these materials. Many researchers have studied the damage process and found interesting results within the continuum mechanics theory using the plasticity framework. An example of this approach can be found in the classical book by [1] and the revised edition by [2] and [3]. An alternative perspective considers the value of incorporating the random nature of material properties and using Discrete Methods as alternative strategies. The technical literature offers several Discrete Element approaches, including two literature review papers [4], [5].

To solve the problem, considering the mechanical collapse governed by fracture as a phase transition problem could be interesting. This approach is commonly used in Statistical Physics, as presented in classical books such as [6]. Many prestigious researchers in Solid Mechanics also support this point of view, including [7], [8], and [9].

As an example of phase transition problems, it is possible to cite the state change from solid to liquid or from ferromagnetic to paramagnetic at characteristic temperatures. In these problems, the phase transition occurs at a critical temperature and the function governing this process near this critical value exhibits a particular behaviour. In the theoretical framework of statistical physics, this parameter is referred to as the control parameter (CP). On the other hand, another typical parameter is the 'Order Parameter' (OP), a global parameter that changes significantly when the CP reaches its critical value. The OP represents the density in the change of state transition problem and the magnetization in the other example cited. The interesting point of this approach is that when the system is close to the critical CP, the parameters that govern the system follow a potential law with characteristic exponents. The physical interpretation of this fact is related to the fact that close to the situation when the phase transition happens, the phenomenon studied doesn´t depend on the boundary conditions and geometry of the specific problem analysed.

The normalization group method proposed by [10] explains this universal behavior. The practical implication of this characteristic behaviour, in the context of the failure of materials, implies that when the system is close to the local or global collapse during its damage process, the global parameters that govern the system follow potential laws with characteristic exponent. Then, when these global parameters adopt a potential shape with a characteristic value, the global or local collapse is imminent.

In [8], a statistical distribution of seismic magnitudes in Japan between 1985 and 1998 is plotted on a log-log axis, revealing a potential law between the number of events and their magnitude. If the entire interval is plotted, a potential expression with an exponent of 0.88 is clearly visible, as depicted in Fig. 1(a). However, reducing the time interval close to a significant seismic event results in an exponent of 0.6. In this case, the interval used to compute the time close to the collapse was [0,100 days]. Within this time window, the statistical distribution of seismic magnitudes is defined by a potential law with an exponent of 0.6. Figure 1(a) illustrates this phenomenon, which was originally presented in [8] and adapted in this work.

In the present work two applications are investigated by using the AET. In the first one the Discrete Element Method is employed in order to simulate a plate under pure shear loading. The second application involves an experimental test of a cracked basalt specimen. Acoustic Emission data is simulated/measured and global parameters are computed in both applications.

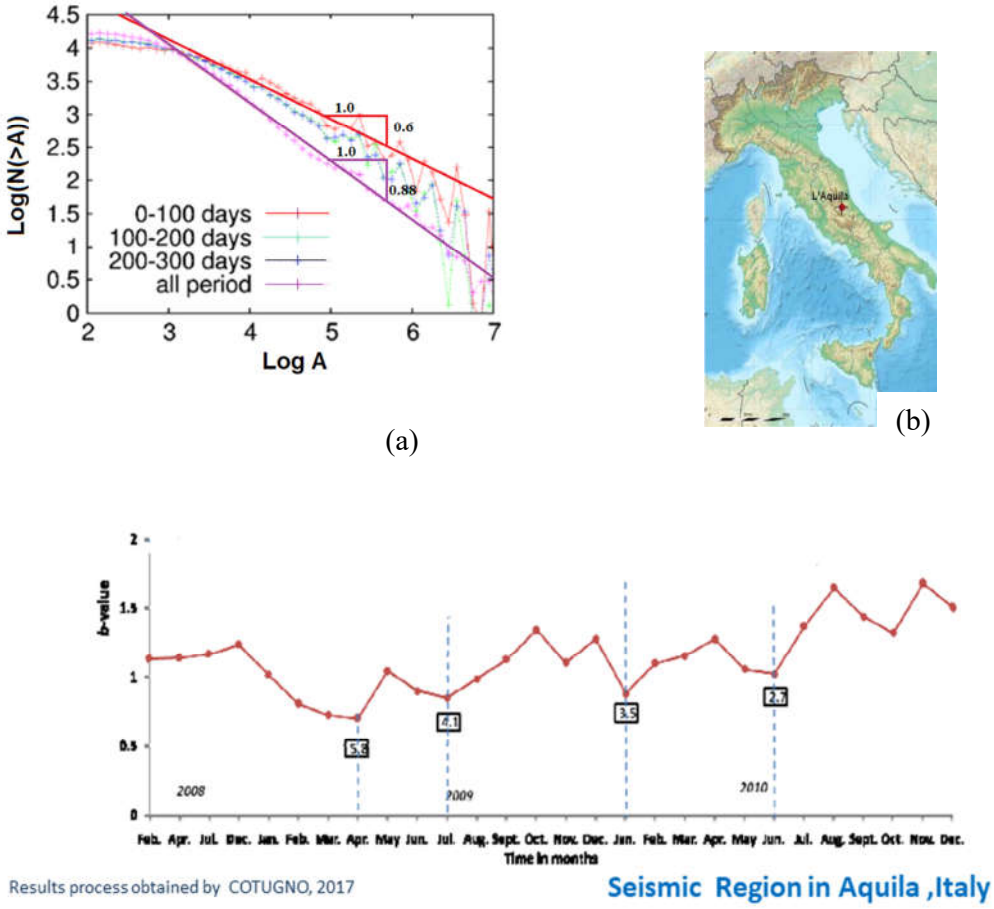

Figure 1: (a) The relation between the events statistical distributions during the seismic evolution in Japan vs their amplitude in the period of [1985-1998]. The exponent change from 0.88 when all the period is considered to 0.6 when a period close to the main shock (day 0) is considered. (b) and (c) the map of Italy with the position of Aquila place where a strong earthquake happen in 2009, and the b value evolution obtained using the seismic information of this region. Notice that close before a great activity happen the b value decrease.

2. Tools used in the Analysis

In the following the Acoustic Emission technic and the Discrete Element method used in the simulations are briefly described.

2.1 Acoustic emission technique

The acoustic emission signal allows for the capture of the spatial and temporal distribution of events associated with mechanical changes in the studied body through sensors placed on its surface. A key resource for Acoustical Emission techniques applied to quasi-fragile materials is [11], which is among the extensive technical material developed on this topic over the last sixty years. The researchers proposed several alternatives for computing global parameters using signal information. The most classical method, originally used in seismological applications, was proposed by Gutenberg & Richter and presented in [12]. This law proposes a relation between the number of events (N) and the signal amplitude (A), which can be expressed as follows:

$$N(\geq A) \propto A^{-\mathrm{b}} \tag{1}$$

where N is the cumulative number of events and A is the signal amplitude. The physical meaning of b is discussed in [13]. According to Eq. 1, most events produce signals with small amplitudes. As damage progresses, localization effects occur, and the events preferentially emanate from the micro crack cloud, resulting in macro crack nucleation. In this cases the b value decreases. An example of the practical application of the value b is presented in Cotugno [14], considering the seismic activity of the Aquila region in Italy, Fig. 1(b). Analysis of the b-value over time, Fig. 1(c), shows that close to significant earthquakes the b-value decreases. The b value computation is schematically illustrated in Fig. 2(a) using the approach proposed by Gutenberg Richter [12].

In addition, in this paper it is computed a precursor index proposed by Debsky Pradhan and Hansen [15], named DPH index in the following. This index involves carrying out a temporal derivative of a measured elastic energy during a test. The index was investigated through numerical simulation in reference [15].

The schematic description of the DPH index computation proposed in Hansen in [15] is presented in Fig 2(b).

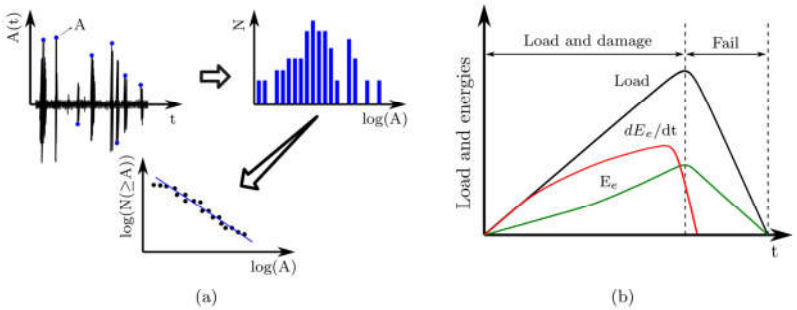

Figure 2: (a) An example of device record vs time, the AE signal statistical density and the accumulated number of signals with the axis in log-log scale where the b value coefficient presented in Eq. 1 appear. (b) The DPH index, represented in schematic form by the red curve.

2.2 The Lattice Discrete Element Method (DEM)

In the present DEM formulation, solid bodies are modelled by means of an arrangement of nodal lumped masses interconnected by massless uniaxial elements able to carry only axial loads. Nayfeh and Hefzy [16] determined the properties of an orthotropic elastic continuum equivalent to an arrangement of axial elements, consisting of a cubic cell with nine nodes, as shown in Fig. 3(a). This representation of an orthotropic continuum was adopted by Riera [17] to solve structural dynamic problems. The mass is concentrated at nodal points, each of which has three degrees of freedom (the displacements in the three orthogonal coordinate directions). For the basic geometric arrangement used herein, the lengths of longitudinal and diagonal elements are L_n and $L_d = \sqrt{3L/2}$, respectively. The equations that relate the equivalent elements stiffness and the properties of an isotropic elastic solid are presented as follows,

$$EA_n = E\phi L^2, \qquad EA_d = \frac{A_o 2\sqrt{3}}{3}, \tag{2}$$

where Young's module is denoted by E, L is the length of longitudinal elements, $\phi = (9 + 8\delta)/(18 + 24\delta)$ and $\delta = 9\nu/(4 - 8\nu)$ are coefficients that relate the parameters, defined for longitudinal and diagonal elements, with the linearly elastic solid properties. Poisson's coefficient ν appears in the definition of factor δ. The DEM model used herein is completely equivalent to an isotropic elastic solid when $\nu = 0.25$. The spatial discretization results in N equations of motion, in which internal material damping is assumed a linear

function of the velocities of nodal masses. The resulting equations of motion may be written in the well-known form,

$$\boldsymbol{M\ddot{u}} + \boldsymbol{C\dot{u}} + \boldsymbol{F_r}(t) - \boldsymbol{P}(t) = \boldsymbol{0} \tag{3}$$

where $\boldsymbol{u}$ represents the vector of generalized nodal displacements, $\dot{\boldsymbol{u}}$ denotes the temporal derivative of $\boldsymbol{u}$, $\boldsymbol{M}$ the diagonal mass matrix, $\boldsymbol{C}$ the damping matrix, both assumed diagonals, $\boldsymbol{F_r}(t)$ the vector of internal forces acting on the nodal masses and $\boldsymbol{P}(t)$ the vector of external forces. Obviously, if $\boldsymbol{M}$ and $\boldsymbol{C}$ are diagonal, Eq. 3 is not coupled.

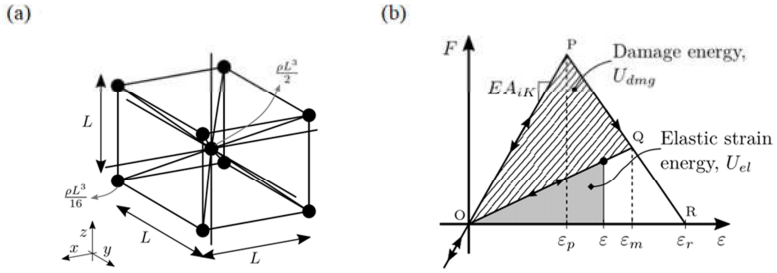

Figure 3: View of basic DEM model: (a) the basic cubic module, (b) Constitutive law adopted for DEM uniaxial elements.

For fracture analysis, the softening law for quasi-brittle materials proposed by Hillerborg [18] was adopted. It is thus assumed that the force-strain relation for elements subjected to tension is defined by the triangular constitutive relationship presented in Fig. 3(b), which allows accounting for the irreversible effects of crack nucleation and propagation. The area under the force vs. strain curve (the area of the triangle OPR) is related to the energy density necessary to fracture the area of influence of the element. Thus, for a given point P on the force vs. strain curve, the area of the triangle OPQ quantifies the energy density dissipated by damage. Once the damage energy density equals the fracture energy, the element fails and loses its load carrying capacity. On the other hand, under compression the material was assumed linearly elastic. Thus, failure in compression is induced by indirect tension.

Constitutive parameters and symbols are defined below: the element axial force F depends on the axial strain ε. An equivalent fracture area A_i^* of each element is defined in order to satisfy the condition that the energy dissipated by fracture of the continuum and by its discrete representation are equivalent. With this purpose, fracture of a cubic sample of dimensions $L \times L \times L$ is considered. The energy dissipated by fracture of a continuum cube due to a crack parallel to one of its faces is $\Gamma = G_f \Lambda = G_f L^2$, in which Λ is the actual fractured area, i.e., L^2. On the other hand, the energy dissipated when a DEM module of dimensions $L \times L \times L$ fractures in two parts consists of the contributions of five longitudinal elements (four coincident with the module edges and an internal element) and four diagonal elements.

The strains ε_p and ε_r (see Fig. 3(b)) are related to another material parameter, the characteristic length d_{eq}, by means of the equations,

$$\varepsilon_p = \sqrt{\frac{G_f}{E d_{eq}}}\ , \quad \varepsilon_r = \varepsilon_p d_{eq} \left(\frac{A_i^*}{A_i}\right)\left(\frac{2}{L_i}\right), \tag{4}$$

in which A^* denotes the equivalent fracture area of each element defined to accomplish that the energy dissipated by fracture of the continuum and by its discrete representation are the same. The subindex i identifies the type of element referenced (diagonal or normal).

Unstable fracture propagation, requires that the characteristic length of the structure, d_{eq}, should be exceeded. The characteristic length is especially relevant because it represents the minimum crack dimension for an unstable fracture to start unstable propagating. d_{eq} could be relate to the dimensionless stress brittleness number, *s*, proposed by Carpinteri [19] defined as $s=[(G_cE/d)^{0.5}/\sigma_p]$. Where d represents the structure's characteristic length and σ_p is the failure stress. Combining the expression of ε_p presented in (4) and considering $\sigma_p=E\varepsilon_p$, it is possible rewrite *s* as $s=(d_{eq}/d)^{0.5}$. These relations are discussed in more detail in [20] and [21].

3. Applications

3.1 First application: AE events from a simulated fracture process using DEM

As a first application, we evaluate the proposed DEM approach through a simulated test. The test involves the fracture process of a square plate subjected to prescribed displacements, inducing a nominally homogeneous pure-shear load with linearly increasing amplitude. We evaluate the corresponding damage process through virtual AE events generated by the acceleration waves induced within the structure as cracks occur.

This simulation refers to a concrete-made, 316 mm-long, and 36 mm-thick square plate, shown in Fig. 4(a) with its prescribed boundary conditions. The figure also includes the positions of virtual AE sensors, simulating accelerometers aligned with the direction normal to the plate's median plane. The corresponding DEM model comprises $79 \times 79 \times 9$ cubic cells, with $L_n = 4$ mm.

In Table 1, d_{eq}=0.022 m was obtained by assuming σ_t=10MPa as σ_p, G_f=70N/m, E=32GPa, and *d*=0.316m. In this case the stress brittleness number proposed by Carpinteri could be computed as *s*=0.27, and combining *d* and *s* could be used to compute d_{eq}.

For the random field, the DEM elements' coefficient of variation is determined according to [22], which has shown that $CV_{Gfsolid}=CV_{Gf}/2.5$ for the DEM's cubic arrangement. Thus, $CV_{Gfsolid}=100\%/2.5=40\%$ in the present case. The correlation lengths l_{cx}, l_{cy}, l_{cz} are considered equal to the cubic module's side. Random mesh variability is also introduced as normally-distributed perturbation with CV_p=2.5%. The introduction of randomness in the DEM is discussed in more general terms in [23].

Table 1. DEM parameters and material properties of the plate.

μ_{G_f}	CV_{G_f}	CV_p	E	d_{eq}	ρ	ν	L_n	l_c
$70\ N/m$	100%	2.50%	$32\ GPa$	$0.020\ m$	$2400\ kg/m^3$	0.25	$4\ mm$	$4\ mm$

Fig. 4(a) illustrates the same test regarding the shear stresses along each plate edge as function of the distortion angle. The behaviour is approximately linear until the peak load is reached. Then, unstable fracture propagation takes place, leading to large changes in the stress distribution. Notice that the test concentrates on the damage process leading to collapse, so the post-peak behaviour is not considered. The corresponding energy balance appears in Fig. 4(b). The sudden raises in kinetic and dissipated energies occurring after the normalized time of 0.8 are clear indicators of unstable growth in the main crack nucleated during the damage process.

In Fig. 5 (top), the final fracture configuration shows a main diagonal cack throughout the plate, which is typical for this kind of test. That information is complemented by the distribution of bars that exceeded their limit strain ε_r, from the start of the process to immediately before the main fracture occurred. In this Figure a distinctly dense cluster of broken bars (a crack) appears where the main crack begins. Such region's dimensions are nearly 0.022 m, which is coherent with the value of d_{eq} i.e., the critical crack size that

generates unstable propagation throughout the specimen. In Fig. 5 **(bottom)** the b value evolution is presented indicating a clear drop of its value when the specimen is in critical regime. More details about the present applications could be seen in [24].

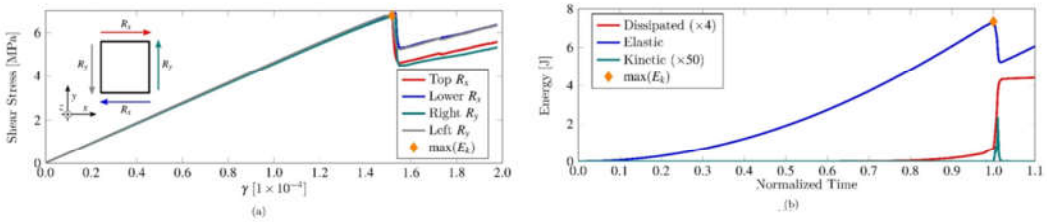

Figure 4: (a) Global shear stress vs. global distortion obtained with DEM. (b) global energy balance.

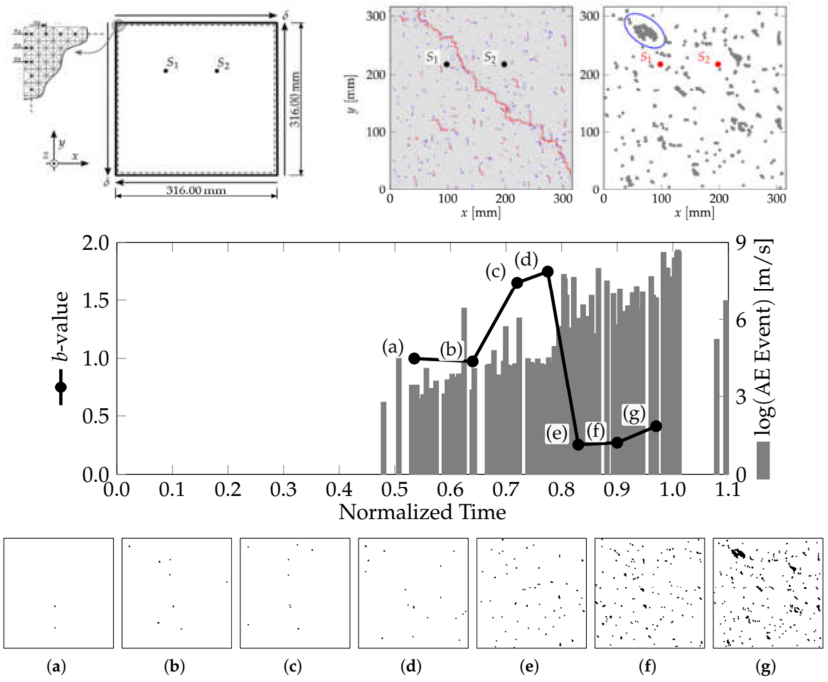

Figure 5: (top) model of the plate submitted to pure shear stress, with boundary conditions and AE sensors positions. Final configuration obtained with DEM model submitted to pure shear test. Broken elements are in red. Spatial distribution of bars where the strain exceeded *εr* from the beginning to immediately before the main fracture occurred. The ellipse indicates where the main crack started. (bottom) Correlation of *b*-value variations with the AE amplitude distribution during the simulated fracture process.

3.2 Second application: Prismatic specimen with oblique Crack

In this application a prismatic specimen with an oblique pre-crack was tested. Fig. 6 **(left)** shows the dimensions, boundary conditions, and specimen failure configuration obtained during the test. The experiment was performed on a basalt sample, seeking to ensure a mixed state of stresses at the tip of the pre-crack. The specimen was subjected to a partial compression load according to the arrangement showed in (see Fig. 6 (top right)), in which the moving parts applied a prescribed displacement at a constant velocity of 0.6 mm/min through a Shimadzu AGX-PLUS universal testing machine. AE measurements were performed with a data acquisition (DAQ) frequency of 455 kHz by using two piezoelectric crystals on the opposite sides of the specimen. The signals were acquired during 290 s, obtaining 1274 hits in the signals post-processing. The adjustment of the boundary conditions applied during the test induced a complex and unanticipated damage pattern. This fact gives an excellent opportunity to assess a damaging process with three local instabilities before reaching global failure (see Fig. 6 (bottom right)). Fig. 7(a) shows the

temporal evolution of the AE parameters calculated from the data collected during the experiment. The time scale is normalized with respect to the rupture time (216.49 s). The graph on top illustrates the load evolution (in red) accompanied by the AE measurements from sensor S_1. Since the measurements from both sensors were very similar, only one data set was used in the remainder of the work. The second graph concerns the *b*-value parameter computed from the mentioned sensor's signals using windows of 35samples with three-sample overlaps. Finally, the bottom graph presents the evolution of the DPH parameter, inferred by taking the time derivative of the product between the applied displacement and the measured reaction forces on the specimen's supports. The three plots presented in Fig.7(a) (top, middle, and bottom) are divided into four different intervals by lightly colored shadows, identified as (I) red, (II) green, (III) blue, and (IV) gray, corresponding to each characteristic behavior identified visually during the test. Fig. 7(b) assists in the interpretation of the damage evolution during the test. The evolution of the b value and the DPH index presented in Fig 7(a) adopting characteristic values, that is falls in the b value and local maxima in the DPH index during the test. More details about this example could be founded in [25].

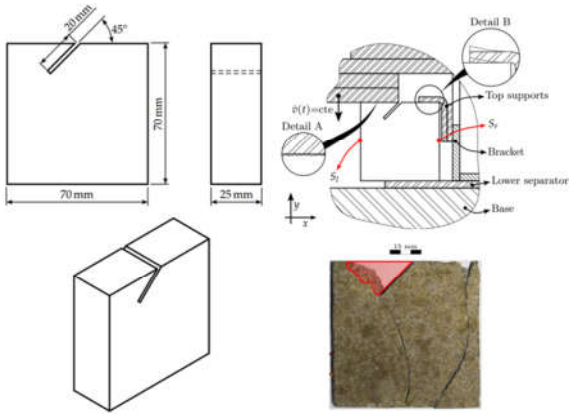

Figure 6: The layout and main dimensions of the basalt specimen test. (left) The specimen dimension. (top right) The dispositive used to fix the basalt specimen during the test. (bottom right) The final configuration obtained.

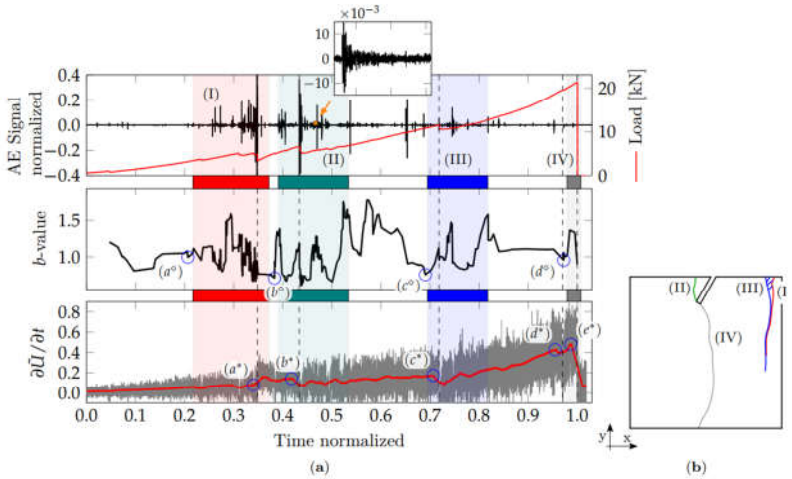

Figure 7: (a) AE experimental results: top—the results of the temporal evolution of Load, Signal AE; middle—*b*-value evolution; bottom—DPH parameter evolution during the test. $(\cdot)^{\diamond}$ and $(\cdot)^{*}$ instants of particular interest for the predictors *b*-value and DPH, respectively. (b) Visual representation of the damage process throughout the test.

4. Conclusions

In the present work, two applications are presented in order to analyse the damage process evolution in quasi-brittle materials using the AE technique. The first is a numerical simulation using a version of the Discrete Element Method where a plate was submitted to a pure shear loading, and the second is an experimental test where a prismatic pre-cracked basalt specimen is loaded until the collapse. The analysis of both examples is carried out by means of global parameters computed based on the AE data obtained for the case of the b value, and from the global load - displacement response for the case of the DPH index. In this two applications, it was possible to perceive that the global indexes could be used as precursors to indicate when the structural system enters the critical regime.

Acknowledgements: The authors acknowledge the financial support received from the Brazilian National Council for Scientific and Technological Development (CNPq) and from Coordination for the Improvement of Higher Education Personnel (CAPES).

References

[1] Kachanov LM. Introduction to Continuum Damage Mechanics. In: Mechanics of Elastic Stability. Volume 10. Dordrecht, the Netherlands: Springer; 1986. https://doi.org/10.1007/978-94-017-1957-5.
[2] Park T, Ahmed B, Voyiadjis GZ. A review of continuum damage and plasticity in concrete: Part I—Theoretical framework. Int J Damage Mech. 2022;31:901–954.
[3] Voyiadjis GZ, Ahmed B, Park T. A review of continuum damage and plasticity in concrete: Part II—Numerical framework. Int J Damage Mech. 2022;31:762–794. https://doi.org/10.1177/10567895211063227.
[4] Mastilovic S, Rinaldi A. Two-Dimensional Discrete Damage Models: Discrete Element Methods, Particle Models, and Fractal Theories. In: Voyiadjis G, eds. Handbook of Damage Mechanics. New York, NY: Springer; 2015. pp. 273-303.
[5] Jenabidehkordi A. Computational methods for fracture in rock: a review and recent advances. Front Struct Civ Eng. 2019.
[6] Huang K. Statistical Mechanics. 2nd ed. New York, NY: Wiley; 1987.
[7] Biswas S, Ray P, Chakrabarti BK. Statistical Physics of Fracture, Breakdown, and Earthquake: Effects of Disorder and Heterogeneity. Weinheim, Germany: John Wiley & Sons; 2015.
[8] Kawamura H, Hatano T, Kato N, Biswas S, Chakrabarti BK. Statistical Physics of Fracture, Friction and Earthquake. Rev Mod Phys. 2012;84:839–884.
[9] Rundle JB, Turcotte DL, Shcherbakov R, Klein W, Sammis C. Statistical physics approach to understanding the multiscale dynamics of earthquake fault systems: Statistical physics of Earthquakes. Rev Geophys. 2003;30.
[10] Wilson KG. Problems in Physics with Many Scales of Length. Sci Am. 1979;241:140-157.
[11] Grosse CU, Ohtsu M. Acoustic Emission Testing. Berlin/Heidelberg, Germany: Springer; 2008.
[12] Richter CF. Elementary Seismology. San Francisco and London: W. H. Freeman; 1958.
[13] Carpinteri A, Lacidogna G, Puzzi S. From criticality to final collapse: evolution of the b-value from 1.5 to 1.0. Chaos Soliton Fract. 2009;41:843–853.
[14] Cutugno P. C.: "Space-time correlation of earthquakes and acoustic emission monitoring of historical constructions." Tese de Doutorado. Politécnico de Torino, Truim, Itália. 2016
[15] Dębski W, Pradhan S, Hansen A. Criterion for Imminent Failure During Loading—Discrete Element Method Analysis. Frontiers in Physics. 2021;9.
[16] Nayfeh AH, Hefzy MS. Continuum Modeling of Three-Dimensional Truss-Like Space Structures. AIAA Journal. 1978;16:779–787. https://doi.org/10.2514/3.7581.
[17] Riera JD. Local effects in impact problems on concrete structures. In: Proceedings, conference on structural analysis and design of nuclear power plants. Porto Alegre, RS, Brazil; 1984. Vol. 3, CDU.
[18] Hillerborg A. A model for fracture analysis. Cod LUTVDG/TVBM. 1971;300:51–81.
[19] Carpinteri A. Application of fracture mechanics to concrete structures. Journal of the Structural Division (ASCE). 1982;108(4):833–848.
[20] Kosteski LE, Iturrioz I, Lacidogna G, Carpinteri A. Size effect in heterogeneous materials analyzed through a lattice discrete element method approach. Eng Fract Mech. 2020;232:107041.
[21] Birck G, Rinaldi A, Iturrioz I. The fracture process in quasi-brittle materials simulated using a lattice dynamical model. Fatigue Fract Eng Mater Struct. 2019;42:2709–2724.

[22] Kosteski LE, Barrios D'Ambra R, Iturrioz I. Crack propagation in elastic solids using the truss-like discrete element method. Int J Fract. 2012;174:139.
[23] Puglia VB, Kosteski LE, Riera JD, Iturrioz I. Random field generation of the material Properties in the Lattice Discrete Element Method. Analysis for Eng Design. 2019;54(4).
[24] Tanzi BN Rojo, Birck G, Sobczyk M, Iturrioz I, Lacidogna G. Truss-like Discrete Element Method Applied to Damage Process Simulation in Quasi-Brittle Materials. Appl Sci-Basel. 2023;13:5119.
[25] Rojo Tanzi BN, Sobczyk M, Iturrioz I, Lacidogna G. Damage Evolution in Quasi-Brittle Materials: Experimental Analysis by AE and Numerical Simulation. Appl Sci. 2023;13:10947.